

Entanglement generation via single-qubit rotations in a teared Hilbert space

Tao Zhang,^{1,*} Zhihao Chi,^{1,*} and Jiazhong Hu^{1,2,†}

¹*Department of Physics and State Key Laboratory of Low Dimensional Quantum Physics, Tsinghua University, Beijing, 100084, China*

²*Frontier Science Center for Quantum Information and Collaborative Innovation Center of Quantum Matter, Beijing, 100084, China*

We propose an efficient yet simple protocol to generate arbitrary symmetric entangled states with only global single-qubit rotations in a teared Hilbert space. The system is based on spin-1/2 qubits in a resonator such as atoms in an optical cavity or superconducting qubits coupled to a metal microwave resonator. By sending light or microwave into the resonator, it induces AC Stark shifts on particular angular-momentum eigenstates (Dicke states) of qubits. Then we are able to generate barriers that hinder transitions between adjacent Dicke states and tear the original Hilbert space into pieces. Therefore, a simple global single-qubit rotation becomes highly non-trivial, and thus generates entanglement among the many-body system. By optimal control of energy shifts on Dicke states, we are able to generate arbitrary symmetric entangled states. We also exemplify that we can create varieties of useful states with near-unity fidelities in only one or very few steps, including W states, spin-squeezed states (SSS), and Greenberger-Horne-Zeilinger (GHZ) states. Particularly, the SSS can be created by only one step with a squeezing parameter $\xi_R^2 \sim 1/N^{0.843}$ approaching the Heisenberg limit (HL). Our finding establishes a way for universal entanglement generations with only single-qubit drivings where all the multiple-qubit controls are integrated into simply switching on/off microwave. It has direct applications in the variational quantum optimizer which is available with existing technology.

I. INTRODUCTION

Entanglement is one of the most essential ingredients in quantum technology, including quantum metrology [1–13], quantum information processing [14–17], and quantum computations [18–20]. It also plays a central role in many practical applications such as quantum dense coding [21–23], quantum teleportation [24–27], and quantum cryptography [28, 29], meanwhile it is enabling more and more quantum algorithms and leading to the quantum advantages [30, 31]. Therefore, finding an efficient way to generate entanglement [32–47] is one particularly important subject in quantum science attracting both theoretical and experimental investigations.

Recently, there are pioneer experimental demonstrations generating varieties of entangled states including SSS [48–52], W states [53–58], and GHZ states [59–62]. In order to apply these helpful entangled states into practical applications, one important issue is how to scale up these entangled states with more particles, which is a highly non-trivial problem. Usually, generation of entanglement requires many-body interaction between particles, and extremely high control precision of interaction is needed when the particle number increases. Any imperfection that can be ignored at small system size may deteriorate the fidelity when the particle number scales up. This limits the applicability of entanglement generation and only some particular classes of entangled states are created so far.

Here, we propose a scheme to generate arbitrary symmetric entangled states by only global single-qubit rotations in a teared Hilbert space. The description of symmetric corresponds to a state with the maximal total angular momentum which is on the surface of a Bloch sphere. The physical system is based on spin-1/2 qubits in a high cooperativity (such as 200) resonator. Due to the high cooperativity and nonlinearity of resonators, the resonant frequency is highly influenced by the angular momentum of qubits. Each eigenstate of the angular momentum (Dicke state [63]) corresponds to one particular resonant frequency. By sending light or microwave with different frequencies, the Hilbert space of qubits is teared into pieces. Under this condition, even a global single-qubit rotation to all qubits can induce strong entanglement among the whole ensemble. In this manuscript, we will mathematically prove the capability to generate arbitrary symmetric states and show a few examples on creating famous entangled states with our scheme, such as Dicke states, GHZ states, and SSS. All these states only require very few steps to reach a high fidelity above 99%. Meanwhile, the SSS only need one sequence to have a squeezing factor $\xi_R^2 \sim 1/N^{0.843}$ which is close to the HL and useful in metrology. Particularly, the high cooperativity system has been achieved in varieties of platforms, including the atom-optical cavity systems and the superconducting qubits. Currently, the cooperativity η in the atom-optical cavity system is close to 200 [64]. In superconducting system, the cooperativity η is even higher. A transmission line connecting to gatemon qubits can have an η larger than 400 [65], and a 3D microwave superconducting cavity containing qubits has an η large than 10^6 [66–68]. These recent demonstrations suggest our scheme is actually practical and can be experimentally realized.

* These authors contribute equally to this work.

† hujiazhong01@ultracold.cn

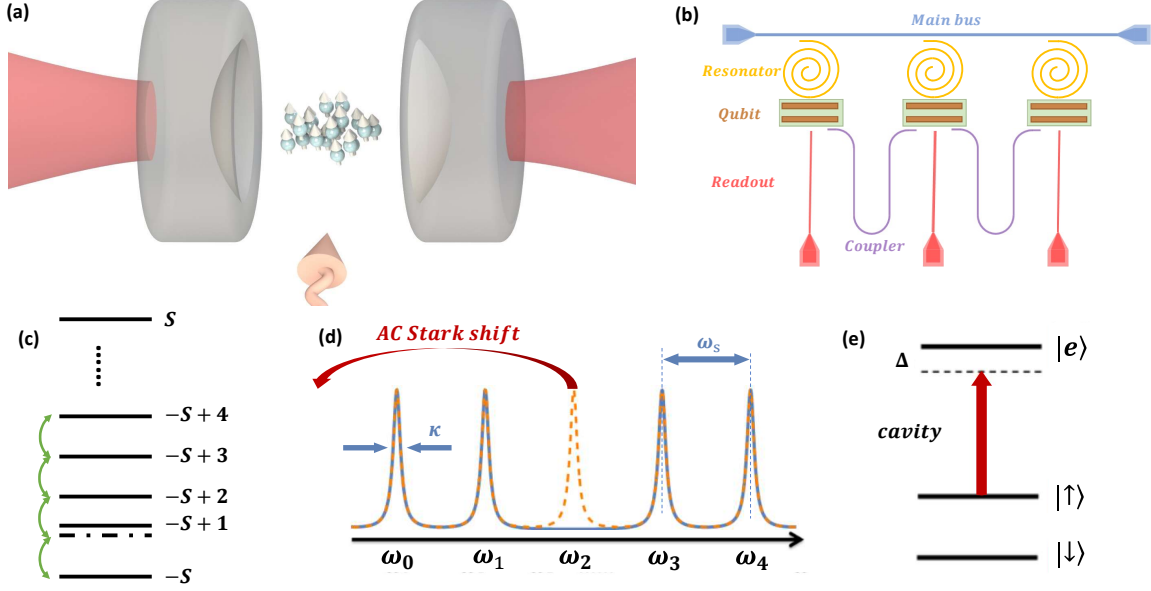


FIG. 1. Setups for entanglement generation via single-qubit rotations in a teared Hilbert space. (a) corresponds to atoms in a cavity and (b) corresponds to superconducting qubits. (c) Dicke state energy levels where one particular Dicke state such as $|-S+1\rangle$ is shifted away and becomes off-resonant. (d) shows the resonant frequency of the resonator is strongly depending on the qubits' populations. Each qubit in $|\uparrow\rangle$ shifts the cavity resonance by an amount of $\omega_s = g^2/\Delta$. When ω_s is larger than the resonator's linewidth κ , each spectrum will be resolved. By sending light or microwave to the resonator with one particular frequency, we can shift only one particular Dicke level away from its original location in the energy spectrum. (e) The energy level of one qubit. The quantized field couples $|\uparrow\rangle$ to the excited state $|e\rangle$ with a detuning Δ .

II. THE SYSTEM DESIGN

We consider N three-level qubits with two ground states $|\downarrow\rangle, |\uparrow\rangle$, and an excited state $|e\rangle$, trapped in a resonator (Fig. 1). The two ground states of each qubit correspond to a spin-1/2 system with $s_i = 1/2$, and we define the collective spin operator as $\hat{\mathbf{S}} \equiv \sum_i \hat{\mathbf{s}}_i$. The resonator mode couples one of the ground states $|\uparrow\rangle$ to the excited state $|e\rangle$ with a detuning Δ and a single-photon Rabi frequency $2g$. The system Hamiltonian is written as

$$\frac{H'}{\hbar} = \sum_i (\omega_0 \hat{s}_{i,z} - \Delta |e\rangle_i \langle e|_i + g \hat{c}^\dagger |\uparrow\rangle_i \langle e|_i + g \hat{c} |e\rangle_i \langle \uparrow|_i), \quad (1)$$

where ω_0 is the energy splitting between $|\downarrow\rangle$ and $|\uparrow\rangle$. \hat{c}^\dagger and \hat{c} are the creation and annihilation operators of the quantized resonator field. By adiabatically eliminating the excited state $|e\rangle$ and converting into the interaction picture, the effective Hamiltonian describing the interaction between the resonator field and N spin-1/2 qubits is written as [69]:

$$\frac{H}{\hbar} = \omega_s (\hat{S}_z + S) \hat{c}^\dagger \hat{c}, \quad (2)$$

where $\omega_s = g^2/\Delta$ is the coupling strength, and $S = N/2$ is the total angular momentum number. This Hamilto-

nian exactly describes the many-body interaction in the cavity quantum electrodynamics regime. In the following texts, we may use the term of *cavity* to refer the resonator and the term of *light* to refer the incident light, microwave, or other-frequency electromagnetic fields of the resonator for the words simplicity.

This interaction term can be interpreted as each qubit in the state $|\uparrow\rangle$ shifts the cavity resonance ω_c by an amount of ω_s , or alternatively the intra-cavity light shifts the energy of each Dicke state by $(S_z + S)\hbar\omega_s \langle \hat{c}^\dagger \hat{c} \rangle$. When the cavity is illuminated by a monochromatic light beam at the frequency $\omega_n = \omega_c + n\omega_s$, the intra-cavity intensity $\langle \hat{c}^\dagger \hat{c} \rangle_{m,n}$ is negligibly small if $m \neq n$ for m qubits in $|\uparrow\rangle$. Therefore, only the state with n qubits in $|\uparrow\rangle$ experiences a significant intra-cavity intensity. Then the Dicke state $|S, S_z = -S + n\rangle$ will be shifted by the AC-Stark shift with an amount of $n\hbar\omega_s \langle \hat{c}^\dagger \hat{c} \rangle_{n,n}$ while the other Dicke states have almost no AC-Stark shift. Therefore, by utilizing this nonlinear property of the cavity system, we can create a Hamiltonian for the qubit ensemble with a form $H_{AC}(n) = \text{Diag}\{0, \dots, 0, C_n, 0, \dots\}$ where there is only one non-zero element on the diagonal $(n+1)$ -th term. Here the matrix is labeled by the Dicke state $|S, S_z = -S + m\rangle$ with an index m .

Now we consider the case of applying a global single-qubit rotation such as $\Omega \hat{S}_x$ and this can be simply achieved by applying a microwave coupling two energy

levels of either atoms or superconducting qubits. If there is no cavity incident light, the rotation term $e^{-i\Omega\hat{S}_x t}$ will rotate the wave function on the surface of the Bloch sphere and this is a trivial scenario where no entanglement will be introduced (Fig. 2a and b). If there is a light with the frequency ω_n , there will be a barrier at the location of $|S, -S + n\rangle$ on the Bloch sphere because this particular Dicke state is shifted away. When the wave function is rotated approaching the state $|S, -S + n\rangle$, it cannot fully penetrate into this barrier and has to be distorted and turn around on the Bloch sphere (Fig. 2c and d). In fact, this light is tearing the original Hilbert space into pieces and then the single-qubit rotation under the light on $e^{-i(H_{AC}(n) + \Omega\hat{S}_x)t}$ becomes highly non-trivial near the teared boundary. Thus, the entanglement emerges near this boundary.

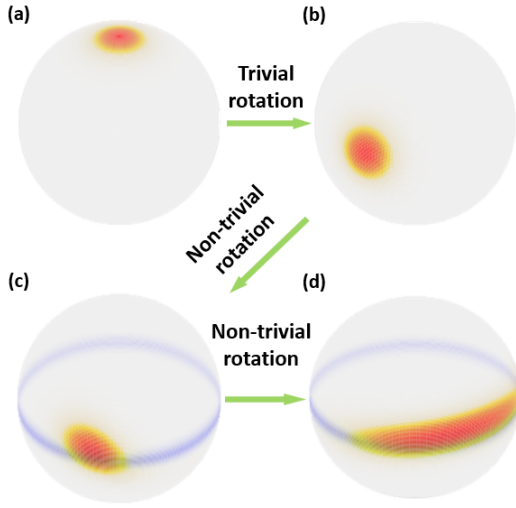


FIG. 2. The illustration of how wave functions evolve represented by the Husimi-Q functions on the Bloch sphere with $N = 50$. (a) A CSS is initialized in $|\downarrow\rangle^{\otimes N}$. (b) A trivial rotation rotates the CSS approaching the boundary shown as a blue stripe in (c) and (d). (c) Applying the non-trivial rotation, the wave function cannot penetrate the blue stripe and it has to be distorted. (d) Continuing the rotation, the wave function is highly squeezed around the blue stripe and the entanglement is created.

III. CREATING ENTANGLEMENT VIA NON-TRIVIAL ROTATIONS

In this section, we describe the details how we create arbitrary symmetric entangled states, and also the considerations of real experimental situations with finite cooperativity, cavity linewidth, and qubit decoherence from the spontaneous decay. Here, each qubit has a spontaneous decay rate Γ in the excited state $|e\rangle$ and the cavity also has a finite linewidth κ . For a monochromatic incident light with a frequency $\omega_l = \omega_c + \delta$, the cavity amplitude transmission function for n qubits in $|\uparrow\rangle$ is given

by [69, 70]

$$\mathcal{T}(\delta, n) = \frac{1}{1 + \frac{n\eta}{1+4(\Delta+\delta)^2/\Gamma^2} - 2i \left[\frac{\delta}{\kappa} - n\eta \frac{(\Delta+\delta)/\Gamma}{1+4(\Delta+\delta)^2/\Gamma^2} \right]}. \quad (3)$$

Here, $\eta = 4g^2/(\Gamma\kappa)$ is the cooperativity while the angular momentum S_z is $S_z = -S + n$. This formula has included the spontaneous emission into the free space which will also lead to a broadening of the cavity linewidth. Note that we have assumed $|\Delta| \gg \Gamma$ and $|\Delta| \gg |\delta|$, i.e. the $|\downarrow\rangle$ state is off-resonant with the cavity mode. Generally, qubits on $|\downarrow\rangle$ state also contribute to scattering events during the evolution, which will be taken into consideration in the followings during the numerical calculations.

When $\omega_s = g^2/\Delta$ is larger than κ , the shifted cavity lineshape under each Dicke state $|S, -S + n\rangle$ is resolved where transmission spectrums do not overlap with each other. Therefore, the intra-cavity light intensity will be negligibly small if we choose $\delta = m\omega_s$ with $m \neq n$. In a practical cavity system with a finite cavity linewidth, a modified non-Hermitian Hamiltonian describes the energy shift of the Dicke states under spontaneous decay of excited states:

$$H_{AC}(\delta, C) = C \times \text{Diag}\{0 \times |\mathcal{T}(\delta, 0)|^2, 1 \times |\mathcal{T}(\delta, 1)|^2, 2 \times |\mathcal{T}(\delta, 2)|^2, \dots\} \quad (4)$$

Here $C = \hbar\delta_{AC}(1 - i\frac{\Gamma}{2\Delta}) / |\mathcal{T}(\delta, \delta/\omega_s)|^2$ is a coefficient which is proportional to the incident light intensity. The real part of Eq. 4 characterizes AC Stark shifts for different Dicke states and the imaginary part characterizes the spontaneous-decay-induced decoherence. Besides sending one monochromatic light, we can also use a light with multiple frequencies $\omega_c + \delta_i$. Therefore, the overall Hamiltonian of sending light to the resonator becomes $H_{AC} = \sum_i H_{AC}(\delta_i, C_i)$. Here $\delta_i = n_i\omega_s$ can be chosen from $n_i \in \{0, 1, \dots, N\}$ and then H_{AC} can be tuned as an arbitrary diagonal Hamiltonian by linear combinations of $H_{AC}(\delta_i, C_i)$.

What we did next is just alternatively applying the trivial and non-trivial single-qubit rotations $\Omega\hat{S}_\phi$ of all qubits, corresponding to global single qubit rotation with or without the incident light. Here $\hat{S}_\phi = \hat{S}_x \cos \phi + \hat{S}_y \sin \phi$. First, all N qubits are initialized in $|\downarrow\rangle^{\otimes N}$. Then we use the trivial rotation, and the state is rotated into another coherent spin states (CSS) with a form of $|\text{CSS}\rangle = e^{-i\Omega\hat{S}_{\phi_1}t_1} |\downarrow\rangle^{\otimes N}$. Next we apply the non-trivial rotation. This leads to a new state

$$\begin{aligned} |\psi_1\rangle &= e^{-i[H_{AC,1} + \hat{\Omega}_1\hat{S}_{\phi'_1}]\hat{t}_1} |\text{CSS}\rangle \\ &= e^{-i[H_{AC,1} + \hat{\Omega}_1\hat{S}_{\phi'_1}]\hat{t}_1} e^{-i\Omega\hat{S}_{\phi_1}t_1} |\downarrow\rangle^{\otimes N}. \end{aligned} \quad (5)$$

After one round of the operations, we label this as one sequence with two steps and then we repeat this process again. Each time, we pick up different barrier positions and set different rotation angles or phases. After j -th

sequences, the state $|\psi_j\rangle$ can be written by a recursive form as

$$|\psi_j\rangle = e^{-i[H_{AC,j} + \tilde{\Omega}_j \hat{S}_{\phi'_j}]} \hat{t}_j e^{-i\Omega \hat{S}_{\phi_j} t_j} |\psi_{j-1}\rangle. \quad (6)$$

By repeatedly applying the above sequence with two steps, we are able to approach any target entangled state of total angular momentum $N/2$ with arbitrarily high precision, and we give a mathematical proof in Appendix A based on the representation of the Lie algebra in $SU(N+1)$.

IV. EXAMPLES OF ENTANGLED STATES

While by repeating trivial and non-trivial rotations, we can create any entangled states, most of metrologically useful entangled states can actually be created simply within one or very few steps, and the convergence of fidelity is very fast, which we will exemplify in the following. Within one sequence, the SSS are created with a squeezing parameter close to the results of two-axis twisting squeezing which is the HL. Meanwhile, we can also generate most of entangled states within two or three steps and the fidelity can be higher than 99%.

A. Spin squeezed state

We first take the creation of SSS as an example. We use the Wineland parameter [71] $\xi_R^2 = S(\Delta S_\perp)_{\min}^2 / |\langle \mathbf{S} \rangle|^2$ to characterize the entanglement. Compared with the criterion from Kitagawa and Ueda [72], ξ_R^2 is more strict and robust since it includes the considerations of the curvature of the Bloch sphere. Here, $(\Delta S_\perp)_{\min}^2$ is the minimum of the fluctuation $(\Delta S_\perp)^2 = \langle S_\perp^2 \rangle - \langle S_\perp \rangle^2$ for the spin component perpendicular to the mean spin direction and $|\langle \mathbf{S} \rangle|$ is the mean spin length. To show the power and the robustness of this scheme, we restrict ourselves by creating SSS within only one sequence in the discussions below.

For a resonator with a cooperativity $\eta = 200$, we control the form of diagonal terms via creating multiple frequencies components for the incident light which can be achieved by an electro-optical modulator. We first consider the ideal case without the spontaneous decay Γ , such as Ytterbium atoms in an optical cavity where the spontaneous decay Γ is only 7 mHz. Recent spin squeezing experiments in the optical transition of Ytterbium [52] also supports this treatment. Here we use n_f to label the number of frequencies used in the incident light. To understand this process more intuitively, we plot how the wave function evolves under the H_{AC} term near a certain Dicke states in Fig. 2. It is shown that when the population rotates approaching this boundary, it is stretched into a strip shape, corresponding to a SSS. The whole procedure can be simply written as:

$$|\psi_{SSS}\rangle = e^{-i(\Omega S_x + H_{AC})t_2} \times e^{-i(\Omega S_x)t_1} |\downarrow\rangle^{\otimes N}. \quad (7)$$

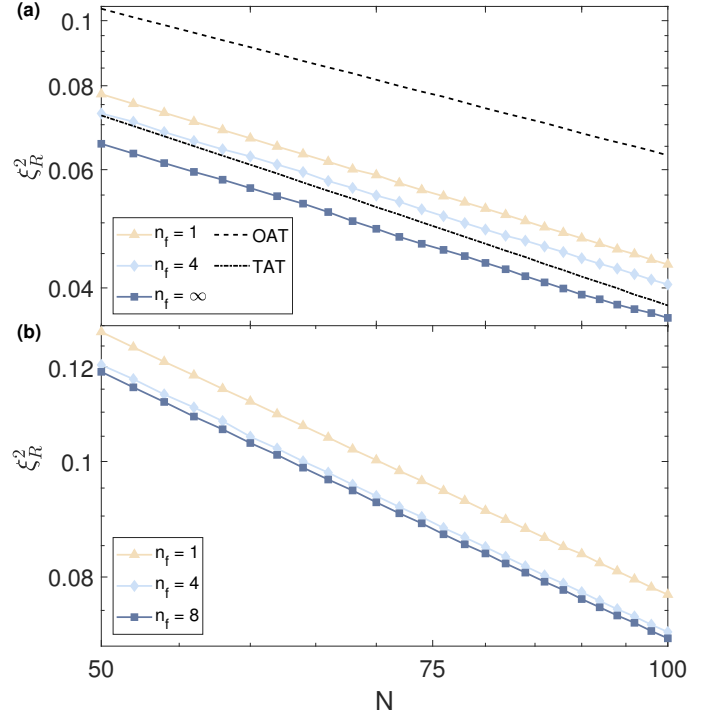


FIG. 3. One sequence squeezing with the squeezing parameter ξ_R^2 versus the qubit number N in the ideal case (a) and ^{87}Rb case with loss (b) with $\eta = 200$. Here we fit ξ_R^2 with a scaling relation $\xi_R^2 = \alpha/N^\beta$. In both panels, n_f is the frequency number in the incident light. $n_f = \infty$ corresponds to arbitrarily chosen diagonal terms in H_{AC} . In panel (a), β equals to 0.843 ($n_f = 1$), 0.851 ($n_f = 4$), and 0.877 ($n_f = \infty$). For comparison, we also plot the relation of $\xi_R^2 \sim 1/N^\beta$ for the OAT and TAT spin squeezing with dashed and dashed-dotted lines, where β equals to 0.724 (OAT) and 0.942 (TAT). In panel (b), the decoherence from incident photon scattering is taken into considerations. The scaling factor β equals 0.731 ($n_f = 1$), 0.745 ($n_f = 4$), and 0.751 ($n_f = 8$).

We show in the Fig. 3(a) the scaling of squeezing parameter ξ_R^2 as a function of total qubit number N under $\eta = 200$. Under the optimized parameters (the optimized parameters can be found in Appendix B), the squeezing parameter shows a similar power-law scaling $\xi_R^2 = \alpha/N^\beta$ with respect to N for different $n_f = 1$ and 4. Ideally, with large enough n_f , one can approach any form of diagonal term H_{AC} with arbitrary precision by direct numerical fitting, which is also shown by $n_f = \infty$ here. As our numerical calculation reveals, while the offset changes, the scaling factor β only varies slightly from 0.84 to 0.88 with the increasing of n_f . The relation of squeezing parameter ξ_R^2 versus the total qubit number N of the one-axis twisting (OAT) scheme (dashed line) and the two-axis counter-twisting (TAT) scheme (dashed-dotted line with $\beta = 0.94$) are also shown in Fig. 3(a).

Here we perform the exact calculations and global parameters optimizations for N from 50 to 100 in Fig. 3. However, our conclusion still works very well for a large N . We can extrapolate these parameters by fitting data

in small N , e.g. in the range of $N = 50$ to 500 . Once we obtain the extrapolated values for a large N , we only need to perform local optimizations and the optimized ξ_R^2 exactly matches the relation in Fig. 3(a) and Fig. 4. We extrapolate the optimized parameters and the scaling relation of ξ_R^2 . Then, we also calculate the corresponding ξ_R^2 for $N = 1000$ by local optimization, and the results also matches the extrapolation. Therefore, our scheme is scalable for generating SSS and the squeezing parameter is better than OAT and close to TAT, i.e. HL, meanwhile this scheme only needs very simple control on/off of the cavity fields.

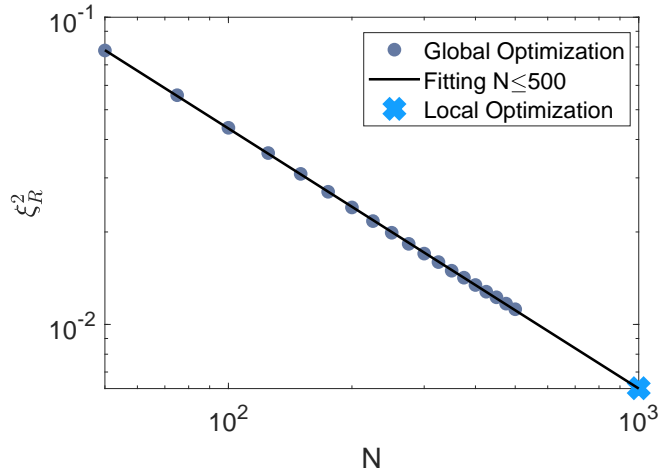


FIG. 4. Spin squeezing scalability. We first find global optimized parameters at $N \leq 500$ (gray dots). Then we fit ξ_R^2 based on data found at $N \leq 500$ (black solid line) and predict ξ_R^2 we can achieve at $N > 500$. To obtain correct parameters for $N > 500$, e.g. $N = 1000$, we fit the optimized parameters found with $N \leq 500$, and conduct local optimizations on these parameters extrapolated from small $N \leq 500$. We find the squeezing parameters ξ_R^2 for large $N = 1000$ (blue cross) matches the extrapolation from $\xi_R^2 \leq 500$.

Furthermore, to show the practical and broad applications of our scheme, we calculate the achievable SSS with a strong spontaneous decay Γ and cooperativity $\eta = 200$. We choose ^{87}Rb , the most common element in atomic clocks and interferometers, as the candidate. Here two $5S_{1/2}$ hyperfine ground states $|\downarrow\rangle = |F=1\rangle$ and $|\uparrow\rangle = |F=2\rangle$ are separated by $2\pi \times 6.8$ GHz, and an excited state $|e\rangle$ in $5P_{3/2}$ has a spontaneous-decay rate $\Gamma = 2\pi \times 6$ MHz. As shown in Fig. 3(b), the optimized squeezing parameter shows similar power-law scaling for different n_f . Different from the ideal-cavity situation above, when the photon scattering appears, one needs to find a balance between further stretching the spin wave function for better ξ_R^2 and the additional variance induced by decoherence from intra-cavity light that deteriorates the metrological gain. But when Δ increases to avoid scattering, cavity light gradually couples both ground states to the excited state. Therefore, we need to include the corrections of the state $|\downarrow\rangle$ to Eq. 2 and 3 in the numerical calculations. When the loss or decoher-

ence is taken into account, the scaling factor β is robust and only decreases a little. The detail parameters and the calculations can be found in Appendix. B. The parameter Δ is fixed during the optimization process, and further enhancement on the squeezing parameter can be achieved by adding Δ into the optimization parameter set.

For practical applications against noises, we also include the considerations of stochastic errors in either the light intensity or the evolution time. We numerically model and simulate these two types of errors in Appendix. C. ξ_R^2 under 5% intensity fluctuations changes very slightly which is almost negligible. This supports the robustness of our scheme for spin squeezing.

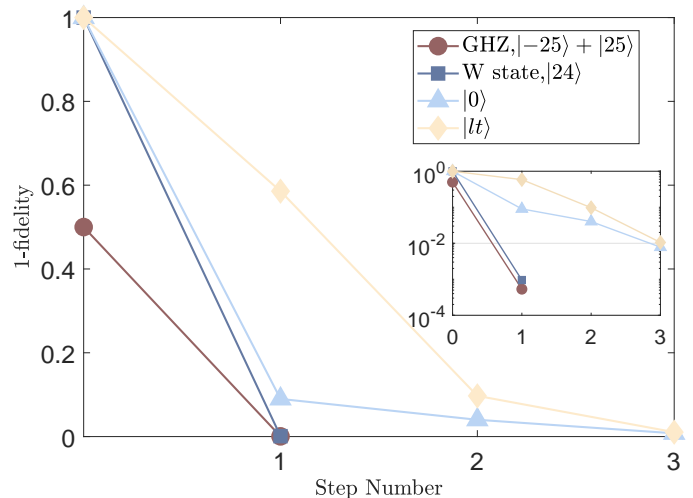


FIG. 5. The entangled-state fidelity versus the step number. The vertical axis is labeled by the difference between 1 and fidelities. The main plot is in a linear scale and the inset is the same data but in a logarithmic scale. Each step contains one non-trivial rotation. Here we use $N = 50$ to demonstrate. The target states include the GHZ state (circle), W state (square), Dicke state $|0\rangle$ (triangle), and lantern state $|lt\rangle$ (diamond). For the GHZ state and W state, within only one step, the fidelity goes over 0.999. For the other two states $|0\rangle$ and $|lt\rangle$, the fidelity goes over 0.99 with three steps.

B. Other entangled states

We now explore the creation of other entangled states. In principle, by repeating applying trivial and non-trivial rotations, our scheme can generate any states on the surface of the N spin-1/2 Bloch sphere. And one can approach a target state at an arbitrarily high fidelity with adequate steps. In this and next sections, we consider the scenario of only sequentially applying non-trivial rotations for numerical calculation simplicity. We use $N = 50$ qubits for demonstrations and we pick up the GHZ state, W state, Dicke state, and lantern state as examples. Using Dicke states $|S_z\rangle$ to express these

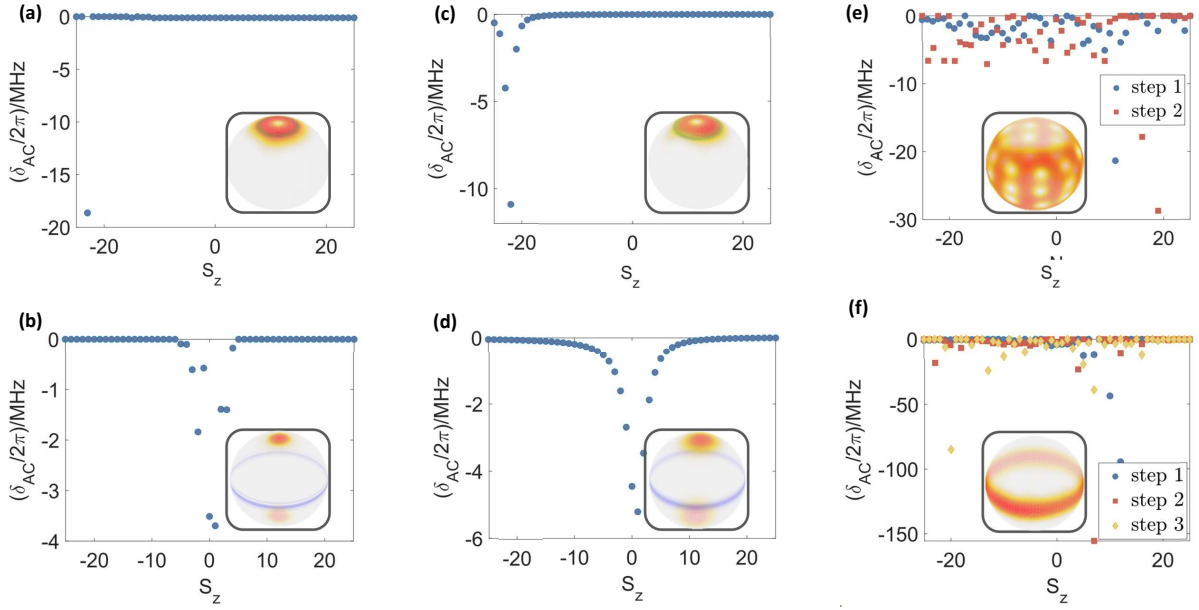


FIG. 6. The form of H_{AC} with corresponding barriers (blue belts) and wave functions on the Bloch spheres with the rotation Rabi-frequency $\Omega = 2\pi \times 0.2$ MHz. The scatter plots show the energy shift for different Dicke states, and the subplots show the result of generated entangled states (Husimi-Q functions) with corresponding barriers used in non-trivial rotations. (a) The ideal situation generating a W state with one step, $t = 0.353\mu s$. (b) The ideal situation generating a GHZ state with one step, $t = 2.49\mu s$. (c) The $\eta = 1000$ ^{87}Rb cavity system generating a W state with one sequence and monochromatic light, $t_1 = 0.151\mu s, t_2 = 0.234\mu s$. (d) The $\eta = 1000$ ^{87}Rb cavity system generating a GHZ state with one sequence and monochromatic light, $t_1 = 0.414\mu s, t_2 = 2.17\mu s$. (e) Two steps generating the lantern state $|lt\rangle = (|-15\rangle + |-5\rangle + |5\rangle + |15\rangle)/2$. Blue and red corresponds to each H_{AC} during the first and second steps, $t = (1.55, 0.305)\mu s$. (f) Three steps generating $|0\rangle$. Blue, red, and orange corresponds to each H_{AC} during the first, second, and third steps, $t = (1.03, 0.318, 0.258)\mu s$.

states, the GHZ state corresponds to $(|-25\rangle + |25\rangle)/\sqrt{2}$, the W state corresponds to $|-24\rangle$, one of Dicke states corresponds to $|0\rangle$, and the lantern state corresponds to $|lt\rangle = (|-15\rangle + |-5\rangle + |5\rangle + |15\rangle)/2$.

In Fig. 5 we plot the fidelities versus the step number. The fidelity of creating a target state increases as we increase total step numbers, where each step only contains a non-trivial step for simplicity. The fidelity rapidly converge to 1 within only very few steps. For the entangled states illustrated, we always obtain a fidelity over 0.99 within 3 steps. Notably, within only one step, a GHZ state with fidelity over 0.999, and a W state with fidelity over 0.99 can be obtained. We will discuss in detail the generation of these two important states in the next section. We plot the wave function of these states and corresponding H_{AC} in Fig. 6. Since the microwave rotation is easy to implement with negligible loss in real experiments, further improvement of the above result includes inserting some trivial rotations between non-trivial ones in order to achieve faster convergence of fidelity approaching unity.

C. GHZ state and W state

In this section, we discuss the generation of the GHZ state and W state more in detail. For GHZ state, we set

the boundary near the equator, i.e. non-zero diagonal terms near $|S_z = 0\rangle$. The intensity of the boundary is set as a weak barrier such that half of the wave function can pass through the barrier and half of the wave function has to be reflected by the barrier (Fig. 7). By continuing the global single-qubit rotations, the transmitted part is rotated into the south pole $|\uparrow\rangle^{\otimes N}$ of the Bloch sphere, and the reflected part takes a U turn around the barrier and comes back to the north pole $|\downarrow\rangle^{\otimes N}$. This leads to a GHZ state, and the boundary here is a quantum analogy of an optical beam splitter. For the creation of W state, one need to set the boundary at $|S_z = -N/2 + 2\rangle$ so that the effective Hilbert subspace consists only of two states, $|S_z = -N/2\rangle$ and $|S_z = -N/2 + 1\rangle$. Under this condition, any global single-qubit rotations will behave like a two-level Rabi oscillation in between these two states.

We show the optimized diagonal terms in the Fig. 6(a) and (b) for creating these two states with only one step. Here we need to utilize multiple-frequency light to engineer the diagonal terms of H_{AC} . Then, we discuss an experimentally-friendly scheme for creating these two states with only monochromatic light (Fig. 6(c) and (d)), where the diagonal terms in H_{AC} are in Lorentzian shape according to Eq. 3. The process of generating the GHZ state is shown in Fig. 7. One can notice that comparing to the most optimized case, the GHZ state generated by monochromatic light is a little tilted, and a trivial

rotation can further improve the fidelity. With the decoherence and loss taken into accounts, the fidelity of GHZ states and W states can be higher than 0.9 and 0.96 with a cooperativity $\eta = 1000$, respectively. Such a cooperativity can be readily achieved in the superconducting qubit system, where $g \sim 100$ MHz, $\Gamma \sim 1$ kHz and resonator with an effective $\kappa \sim 10$ kHz has already been realized in the experiment [66–68]. Since η quantifies the ability to resolve adjacent Dicke states, larger η helps to obtain these two states with a higher fidelity. For large enough η , with single monochromatic light and within one non-trivial rotation, we found the fidelity of the generated GHZ state and W state can reach as high as 0.98 with loss taken into consideration, as shown in Fig. 8. For larger $N = 100$, the achievable fidelity of the GHZ state further increases.

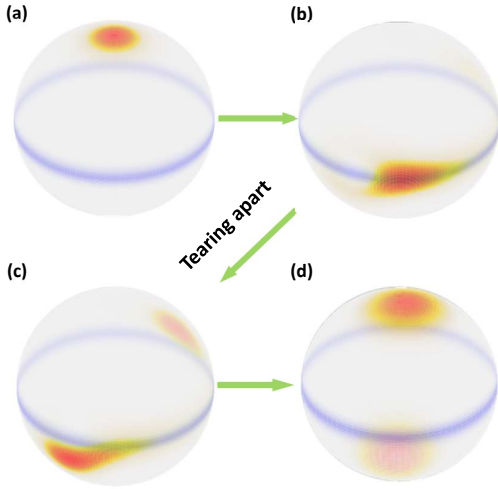


FIG. 7. The illustration of creating a GHZ state represented by the Husimi-Q functions on the Bloch sphere with $N = 50$. (a) A CSS is initialized in $|\downarrow\rangle^{\otimes N}$. (b) A non-trivial rotation directly rotates the CSS approaching to the boundary shown as a blue stripe in each panel, and the boundary starts to tear the wave function. (c) The CSS is torn into two parts while half is transmitted and half is reflected. (d) Continuing the rotation, the wave function is reshaped into the superposition of two opposite CSS, which is a GHZ state.

V. CONCLUSION AND OUTLOOK

In conclusion, we find an efficient yet simple scheme to generate arbitrary symmetric entangled states via single-qubit operations in a teared N spin-1/2 Hilbert space. With currently available technology, we are able to generate any superposition of Dicke states, including spin squeezed states, W states, and GHZ states. This scheme utilize the tearing capability of the intra-cavity light on the Bloch sphere, inducing non-linear interaction among these Dicke states, thus generating highly

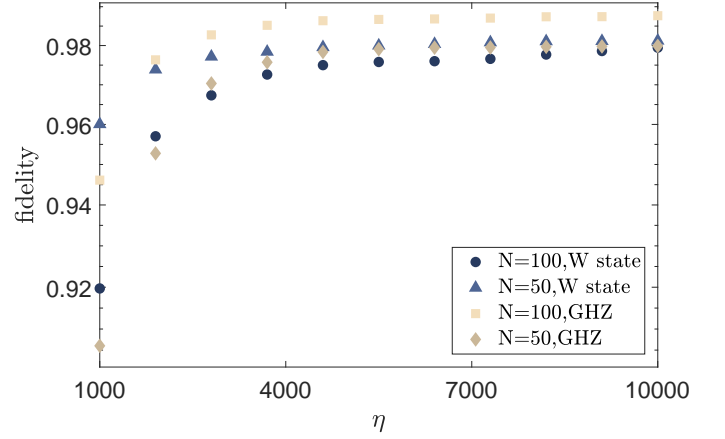


FIG. 8. Fidelity for generating the GHZ state and W state with single monochromatic light by one non-trivial rotation under different cooperativity η and qubit number N . The fidelity of the generated states increases monotonically with η .

entangled states in combination with single-qubit rotation. The only multiple-qubit operation is just switching on/off light or microwave which is practically simple in experiments. We believe our scheme can be of important guidance for experiments in neutral atom-cQED system and superconducting qubits, and variations of this protocol may be used for other system including mechanical oscillators-cavity system and quantum dots ensembles.

VI. ACKNOWLEDGEMENT

This work is supported by National Key Research and Development Program of China (2021YFA0718303, 2021YFA1400904) and National Natural Science Foundation of China (92165203, 61975092, 11974202).

Appendix A: Proof of creating arbitrary states

During the entanglement generations, we are using both trivial and non-trivial rotations with a form of,

$$|\psi_j\rangle = e^{-i[H_{AC,j} + \tilde{\Omega}_j \hat{S}_{\phi'_j}]\tilde{t}_j} e^{-i\Omega \hat{S}_{\phi_j} t_j} |\psi_{j-1}\rangle. \quad (A1)$$

According to the Baker-Campbell-Hausdorff formula, we can rewrite this operation as an effective Hamiltonian H_e with a form of

$$|\psi_j\rangle = e^{-i\Omega \hat{S}_{\phi_j} t_j} e^{-iH_e \tilde{t}_j} |\psi_{j-1}\rangle. \quad (A2)$$

Here H_e is given by

$$H_e = \sum_k \frac{1}{k!} \left[\left(-i\Omega \hat{S}_{\phi_j} t_j \right)^{(k)}, H_{AC,j} + \tilde{\Omega}_j \hat{S}_{\phi'_j} \right], \quad (A3)$$

where $[A^{(k)}, B] = [A, [A^{(k-1)}, B]]$ is a recursive form of commutators. Therefore, we want to prove that the commutators $[S_x^n, H_{AC,j}]$ and $[S_y^n, H_{AC,j}]$ as Lie-algebra can generate the full space of the special unitary Lie group $SU(N+1)$, where n is an integer. This idea is similar to the way in Ref. [73].

Generalized Gell-Mann matrices are the Lie-algebra generators of the special unitary group $SU(N+1)$ which have been clearly studied in the maths [74]. Then our idea converts to that we can use the commutators or their linear combinations to construct this complete set of Gell-Mann matrices. Then based on this, we are able to prove that our operations can lead to any symmetric entangled states under the $SU(N+1)$ form.

First, we would like to give a brief introduction about the formalism of Gell-Mann matrices. Let $E_{(j,k)}$ denote the matrix with a 1 in the (j,k) -th entry and 0 elsewhere. This allows one to define three classes of matrices. The first class is symmetric:

$$\lambda_{(j,k)}^s = E_{(k,j)} + E_{(j,k)}. \quad (A4)$$

The second class is anti-symmetric:

$$\lambda_{(j,k)}^a = -i(E_{(k,j)} - E_{(j,k)}). \quad (A5)$$

The third class only contains diagonal matrices:

$$\lambda_m^D = \sqrt{\frac{2}{m(m-1)}} [E_{(m,m)} - (m-1)E_{(m-1,m-1)}]. \quad (A6)$$

Here the superscripts s , a , and D correspond to symmetric, anti-symmetric, and diagonal. All the matrix in these three classes are one complete set of Gell-Mann matrices.

According to our scheme, it is intuitive to find that the third class of matrices is automatically satisfied by tuning different AC Stark shifts in H_{AC} . Let's define a matrix set $\{Z_m | m \in \mathbb{Z}^+\}$ with a form of $(Z_m)_{(i,j)} = \delta_{i,j} \delta_{i,m}$ where $\delta_{i,j}$ is the Kronecker delta function and it is equivalent to H_{AC} and λ_m^D . Then, let's check the first order commutators,

$$S_x Z_1 - Z_1 S_x = \begin{bmatrix} 0 & -r_1 & \dots & 0 \\ r_1 & 0 & \dots & 0 \\ \vdots & \vdots & \ddots & \vdots \\ 0 & 0 & \dots & 0 \end{bmatrix}, \quad (A7)$$

$$S_y Z_1 - Z_1 S_y = i \begin{bmatrix} 0 & r_1 & \dots & 0 \\ r_1 & 0 & \dots & 0 \\ \vdots & \vdots & \ddots & \vdots \\ 0 & 0 & \dots & 0 \end{bmatrix}, \quad (A8)$$

$$S_x Z_2 - Z_2 S_x = \begin{bmatrix} 0 & r_1 & 0 & \dots & 0 \\ -r_1 & 0 & -r_2 & \dots & 0 \\ 0 & r_2 & 0 & \dots & 0 \\ \vdots & \vdots & \vdots & \ddots & \vdots \\ 0 & 0 & 0 & \dots & 0 \end{bmatrix}, \quad (A9)$$

$$S_y Z_2 - Z_2 S_y = i \begin{bmatrix} 0 & r_1 & 0 & \dots & 0 \\ r_1 & 0 & -r_2 & \dots & 0 \\ 0 & -r_2 & 0 & \dots & 0 \\ \vdots & \vdots & \vdots & \ddots & \vdots \\ 0 & 0 & 0 & \dots & 0 \end{bmatrix}. \quad (A10)$$

Here r_i are real numbers and matrix elements of S_x and S_y . Then by linear combinations of $\{S_x Z_m - Z_m S_x | m \in \mathbb{Z}^+\}$ and $\{S_y Z_m - Z_m S_y | m \in \mathbb{Z}^+\}$, we can construct parts of the first class and the second class of matrices with the restriction of $|i-j|=1$. Now let's check the second-order commutators such as

$$S_x^2 Z_1 - Z_1 S_x^2 = \begin{bmatrix} 0 & 0 & -r_1^2 & \dots & 0 \\ 0 & 0 & 0 & \dots & 0 \\ r_1^2 & 0 & 0 & \dots & 0 \\ \vdots & \vdots & \vdots & \ddots & \vdots \\ 0 & 0 & 0 & \dots & 0 \end{bmatrix}. \quad (A11)$$

Then it is clear that by linear combinations of the second-order commutators $\{S_x^2 Z_m - Z_m S_x^2 | m \in \mathbb{Z}^+\}$ and $\{S_y^2 Z_m - Z_m S_y^2 | m \in \mathbb{Z}^+\}$, we can construct parts of the first and second classes of matrices with the condition of $|i-j|=2$. Utilizing the same arguments, any $\lambda_{(j,k)}^s$ and $\lambda_{(j,k)}^a$ can be constructed. And this proves the completeness of our operations. Therefore, our scheme can lead to any symmetric entangled states connected by the $SU(N+1)$ group.

Appendix B: Spin-squeezed state

In this section, we provide the details about calculating the SSS in both ideal and ^{87}Rb cases.

First we show how we calculate squeezing parameter ξ_R^2 under the Wineland criterion. For a quantum state, we calculate the expectation value of the spin $\langle \hat{\mathbf{S}} \rangle = (\langle \hat{S}_x \rangle, \langle \hat{S}_y \rangle, \langle \hat{S}_z \rangle)$ along different directions. This defines the mean spin direction $\vec{n}(\theta, \phi)$ parallel to $\langle \hat{\mathbf{S}} \rangle$, where $\theta = \arccos(\langle \hat{S}_z \rangle / |\langle \hat{\mathbf{S}} \rangle|)$ and $\phi = \arctan(\langle \hat{S}_y \rangle / \langle \hat{S}_x \rangle)$. We can choose 2 directions \vec{n}_1 , \vec{n}_2 orthogonal to each other and perpendicular to $\vec{n}(\theta, \phi)$, and calculate $C = \langle \hat{S}_{\vec{n}_1}^2 + \hat{S}_{\vec{n}_2}^2 \rangle$, $A = \langle \hat{S}_{\vec{n}_1}^2 - \hat{S}_{\vec{n}_2}^2 \rangle$, and $B = \langle \hat{S}_{\vec{n}_1} \hat{S}_{\vec{n}_2} + \hat{S}_{\vec{n}_2} \hat{S}_{\vec{n}_1} \rangle$. Then the minimum variance of the angular momentum perpendicular to \vec{n} is $v_m = \frac{1}{2}(C - \sqrt{A^2 + B^2})$. Then we calculate the squeezing parameter ξ_R^2 as

$$\xi_R^2 = S v_m / |\langle \hat{\mathbf{S}} \rangle|^2. \quad (B1)$$

Based on Eq. 7 in the main text where we also copy it below,

$$|\psi_{\text{SSS}}\rangle = e^{-i(\Omega S_x + H_{AC})t_2} \times e^{-i(\Omega S_x)t_1} |\downarrow\rangle^{\otimes N}, \quad (B2)$$

the parameters we need to optimize are n_0 , δ_{AC} , t_2 , and t_1 with fixed parameters $\Omega = 2\pi \times 0.2$ MHz and

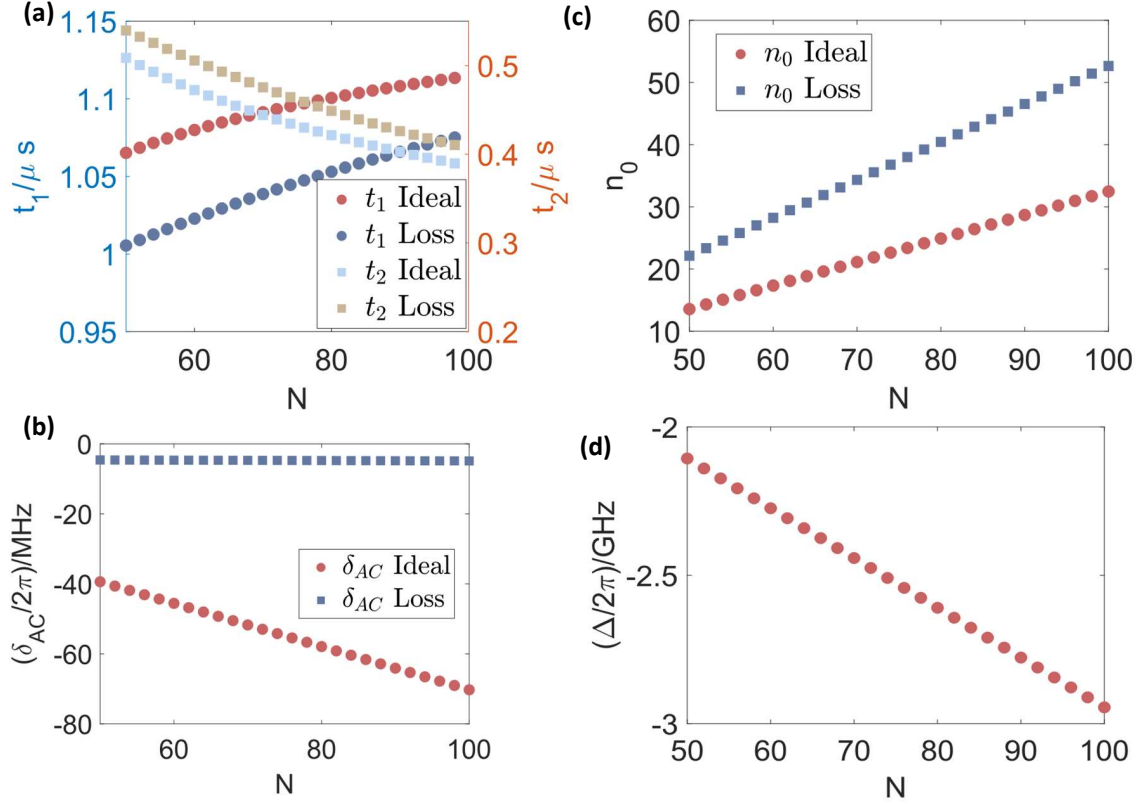


FIG. 9. The globally optimized parameters for N ranging from 50 to 100. In Fig (a), (b), and (c), we show trivial rotation time t_1 , non-trivial rotation time t_2 , δ_{AC} and frequency order parameter n_0 for the ideal case and realistic ^{87}Rb case with loss from the spontaneous decay taken into consideration. (d) corresponds to the optimization of Δ for the realistic ^{87}Rb case.

TABLE I. Fixed parameters for spin squeezing in the ^{87}Rb case

Parameters	Symbol	Number	Unit
Spin Spontaneous Decay Rate	Γ	$2\pi \times 6.06$	GHz
Hyperfine splitting	ω_0	$2\pi \times 6.8$	GHz
Trivial Rotation Angular Velocity	Ω	$2\pi \times 0.2$	MHz
Cooperativity	η	200	

$\Delta = 2\pi \times 0.65$ GHz. Here n_0 corresponds to the light frequency $\omega = \omega_c + n_0\omega_s$. δ_{AC} is the AC Stark shift for the resonant Dicke state. In Fig. 9 (a) to (c), we plot these globally optimized parameters from $N = 50$ to 500. Based on these information, we can extrapolate the optimized SSS parameters for a large N , and the result for large N is consistent with the scaling of the ξ_R^2 for small N , as shown in Fig. 4.

For ^{87}Rb atoms, we consider two $5S_{1/2}$ hyperfine ground states $|\downarrow\rangle = |F=1\rangle$ and $|\uparrow\rangle = |F=2\rangle$, and an excited state $|e\rangle$ in $5P_{3/2}$. Fixed parameters are shown in the Table. I. The hyperfine splitting is 6.8 GHz, and the light coupling between $|\downarrow\rangle$ and $|e\rangle$ must also be included. Therefore, the detuning Δ between $|\uparrow\rangle$ and $|e\rangle$ must be optimized to balance this additional contribution. Then

the Hamiltonian becomes a form like following

$$H_{\text{exp}} = H_{AC}^{\uparrow} + H_{AC}^{\downarrow}. \quad (\text{B3})$$

Here H_{AC}^{\uparrow} and H_{AC}^{\downarrow} corresponds to the AC Stark shift contributed from the states $|\uparrow\rangle$ and $|\downarrow\rangle$.

In order to maintain a better scaling of SSS, the optimal parameters n_0 , δ_{AC} , t_2 , and t_1 must change under the spontaneous decay. Additionally, we need to optimize Δ . We still define the AC Stark shift coefficient for the state $|\uparrow\rangle$ with the form of $C = \hbar\delta_{AC}(1 - \frac{i\Gamma}{\Delta})$ to label out the contribution of light. The influence of $|\downarrow\rangle$ can be easily calculated based on the parameters of $|\uparrow\rangle$ according to the hyperfine splitting. For the contribution of the spontaneous decay, we utilize the method in Ref. [75]. If one qubit is scattered randomly by a photon, it will not contribute to the total spin length anymore. Meanwhile, this randomly reshuffled spin will be in a maximal mixed state after the scattering. Any further coherent evolution does not purify this mixed state anymore. Therefore based on the evolution of a non-Hermitian Hamiltonian for a final state ρ , we are expecting $[1 - \text{Tr}(\rho)]N$ atoms randomly scattered. Therefore the variance contribution becomes

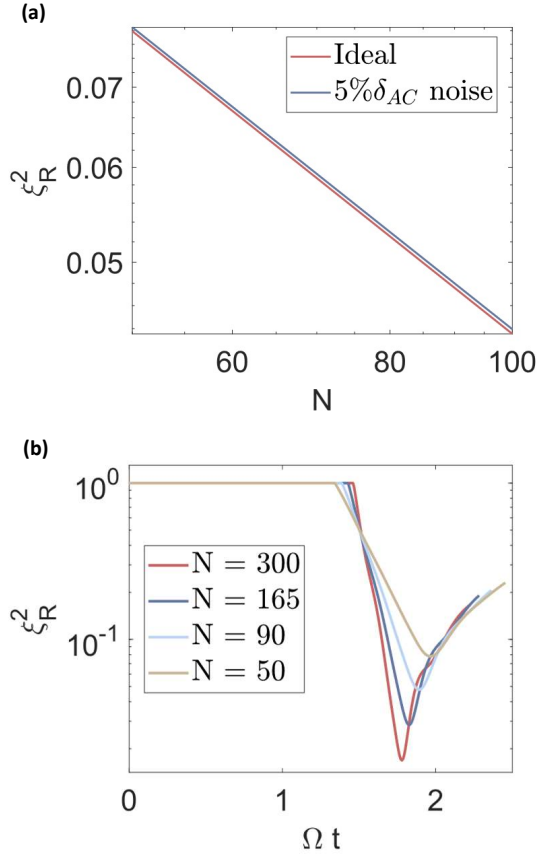


FIG. 10. (a) Simulation of 5% intensity noise effect on ξ_R^2 . (b) The evolution of ξ_R^2 with time.

$v_m + [1 - \text{Tr}(\rho)] N/4$. The squeezing parameter becomes

$$\xi_{R,loss}^2 = S \frac{v_m + [1 - \text{Tr}(\rho)] N/4}{|\langle \hat{S} \rangle|^2}. \quad (\text{B4})$$

In Fig. 9(a) to (d), we show these parameters used in the calculation in the main text Fig. 3.

All these parameters can be obtained online [76].

Appendix C: Experimental imperfections

Imperfections occur when we consider a real experiment, including inhomogeneous coupling, photon shot noise, and cavity instability. Inhomogeneous coupling caused by cavity standing wave can be avoided by using a double-frequency laser. Such as in ^{87}Rb systems, one can use a 780 nm laser to induce the AC Stark shift of Dicke states and a 1560 nm laser to trap atoms. Then, all atoms are trapped to the anti-nodes of lattice as well as the 780 nm light for entanglement. The photon shot noise and the cavity frequency instability randomly change the intra-cavity light intensity, and thus bring fluctuations to AC Stark shifts. Here we simulate this effect with 5% intensity noise in Fig. 10(a), and there is almost no influence from this imperfection.

Then we also consider the relative time accuracy requirement for t_1 and t_2 . As shown in Fig. 10(b), we find that the temporal region corresponding to an SSS becomes narrower as N increases. When N increases, the relative width of a CSS on the Bloch sphere becomes narrower with a scale of $1/\sqrt{N}$. Only when the CSS starts to overlap with the barrier, the squeezing effect appears. Therefore, we have to accurately control the time t_1 and t_2 to exactly force ξ_R^2 sitting at the minimal point. For the scenarios in the main text, any relative time uncertainty below 0.1% can help us to resolve and locate the minimal point of ξ_R^2 which corresponds to 1 ns. To our knowledge, the current microwave atomic clock can safely satisfy these time accuracy requirement.

-
- [1] V. Giovannetti, S. Lloyd, and L. Maccone, Advances in quantum metrology, *Nature photonics* **5**, 222 (2011).
 - [2] L. Pezze, A. Smerzi, M. K. Oberthaler, R. Schmied, and P. Treutlein, Quantum metrology with nonclassical states of atomic ensembles, *Reviews of Modern Physics* **90**, 035005 (2018).
 - [3] C. D. Marciniak, T. Feldker, I. Pogorelov, R. Kaubruegger, D. V. Vasilyev, R. van Bijnen, P. Schindler, P. Zoller, R. Blatt, and T. Monz, Optimal metrology with programmable quantum sensors, *Nature* **603**, 604 (2022).
 - [4] V. Giovannetti, S. Lloyd, and L. Maccone, Quantum metrology, *Physical review letters* **96**, 010401 (2006).
 - [5] P. M. Anisimov, G. M. Raterman, A. Chiruvelli, W. N. Plick, S. D. Huver, H. Lee, and J. P. Dowling, Quantum metrology with two-mode squeezed vacuum: parity detection beats the heisenberg limit, *Physical review letters* **104**, 103602 (2010).
 - [6] B. J. Lawrie, P. D. Lett, A. M. Marino, and R. C. Pooser, Quantum sensing with squeezed light, *Acs Photonics* **6**, 1307 (2019).
 - [7] R. Kaubruegger, P. Silvi, C. Kokail, R. van Bijnen, A. M. Rey, J. Ye, A. M. Kaufman, and P. Zoller, Variational spin-squeezing algorithms on programmable quantum sensors, *Physical review letters* **123**, 260505 (2019).
 - [8] R. Kaubruegger, D. V. Vasilyev, M. Schulte, K. Hammerer, and P. Zoller, Quantum variational optimization of ramsey interferometry and atomic clocks, *Physical review X* **11**, 041045 (2021).
 - [9] E. M. Kessler, P. Komar, M. Bishof, L. Jiang, A. S. Sørensen, J. Ye, and M. D. Lukin, Heisenberg-limited atom clocks based on entangled qubits, *Physical review letters* **112**, 190403 (2014).

- [10] L. Pezzè and A. Smerzi, Heisenberg-limited noisy atomic clock using a hybrid coherent and squeezed state protocol, *Physical Review Letters* **125**, 210503 (2020).
- [11] J. Hu, W. Chen, Z. Vendeiro, A. Urvoy, B. Braverman, and V. Vuletić, Vacuum spin squeezing, *Physical Review A* **96**, 050301 (2017).
- [12] W. Chen, J. Hu, Y. Duan, B. Braverman, H. Zhang, and V. Vuletić, Carving complex many-atom entangled states by single-photon detection, *Physical review letters* **115**, 250502 (2015).
- [13] O. Hosten, R. Krishnakumar, N. J. Engelsens, and M. A. Kasevich, Quantum phase magnification, *Science* **352**, 1552 (2016).
- [14] C. H. Bennett and D. P. DiVincenzo, Quantum information and computation, *nature* **404**, 247 (2000).
- [15] P. Horodecki, L. Rudnicki, and K. Życzkowski, Five open problems in quantum information theory, *PRX Quantum* **3**, 010101 (2022).
- [16] S. Slussarenko and G. J. Pryde, Photonic quantum information processing: A concise review, *Applied Physics Reviews* **6** (2019).
- [17] G. B. Xavier and G. Lima, Quantum information processing with space-division multiplexing optical fibres, *Communications Physics* **3**, 9 (2020).
- [18] T. D. Ladd, F. Jelezko, R. Laflamme, Y. Nakamura, C. Monroe, and J. L. O'Brien, Quantum computers, *nature* **464**, 45 (2010).
- [19] D. P. DiVincenzo, Quantum computation, *Science* **270**, 255 (1995).
- [20] T. Albash and D. A. Lidar, Adiabatic quantum computation, *Reviews of Modern Physics* **90**, 015002 (2018).
- [21] Y. Guo, B.-H. Liu, C.-F. Li, and G.-C. Guo, Advances in quantum dense coding, *Advanced Quantum Technologies* **2**, 1900011 (2019).
- [22] K. Mattle, H. Weinfurter, P. G. Kwiat, and A. Zeilinger, Dense coding in experimental quantum communication, *Physical review letters* **76**, 4656 (1996).
- [23] S. L. Braunstein and H. J. Kimble, Dense coding for continuous variables, *Physical Review A* **61**, 042302 (2000).
- [24] S. Pirandola, J. Eisert, C. Weedbrook, A. Furusawa, and S. L. Braunstein, Advances in quantum teleportation, *Nature photonics* **9**, 641 (2015).
- [25] D. Bouwmeester, J.-W. Pan, K. Mattle, M. Eibl, H. Weinfurter, and A. Zeilinger, Experimental quantum teleportation, *Nature* **390**, 575 (1997).
- [26] X.-X. Xia, Q.-C. Sun, Q. Zhang, and J.-W. Pan, Long distance quantum teleportation, *Quantum Science and Technology* **3**, 014012 (2017).
- [27] X.-M. Hu, Y. Guo, B.-H. Liu, C.-F. Li, and G.-C. Guo, Progress in quantum teleportation, *Nature Reviews Physics* , 1 (2023).
- [28] N. Gisin, G. Ribordy, W. Tittel, and H. Zbinden, Quantum cryptography, *Reviews of modern physics* **74**, 145 (2002).
- [29] C. H. Bennett, F. Bessette, G. Brassard, L. Salvail, and J. Smolin, Experimental quantum cryptography, *Journal of cryptology* **5**, 3 (1992).
- [30] A. J. Daley, I. Bloch, C. Kokail, S. Flannigan, N. Pearson, M. Troyer, and P. Zoller, Practical quantum advantage in quantum simulation, *Nature* **607**, 667 (2022).
- [31] D. Ristè, M. P. Da Silva, C. A. Ryan, A. W. Cross, A. D. Córcoles, J. A. Smolin, J. M. Gambetta, J. M. Chow, and B. R. Johnson, Demonstration of quantum advantage in machine learning, *npj Quantum Information* **3**, 16 (2017).
- [32] R. Horodecki, P. Horodecki, M. Horodecki, and K. Horodecki, Quantum entanglement, *Reviews of modern physics* **81**, 865 (2009).
- [33] M. Erhard, M. Krenn, and A. Zeilinger, Advances in high-dimensional quantum entanglement, *Nature Reviews Physics* **2**, 365 (2020).
- [34] R. McConnell, H. Zhang, J. Hu, S. Čuk, and V. Vuletić, Entanglement with negative wigner function of almost 3,000 atoms heralded by one photon, *Nature* **519**, 439 (2015).
- [35] F. Haas, J. Volz, R. Gehr, J. Reichel, and J. Estève, Entangled states of more than 40 atoms in an optical fiber cavity, *Science* **344**, 180 (2014).
- [36] G. Barontini, L. Hohmann, F. Haas, J. Estève, and J. Reichel, Deterministic generation of multiparticle entanglement by quantum zeno dynamics, *Science* **349**, 1317 (2015).
- [37] A. Kuzmich, K. Mølmer, and E. Polzik, Spin squeezing in an ensemble of atoms illuminated with squeezed light, *Physical review letters* **79**, 4782 (1997).
- [38] T. Fernholz, H. Krauter, K. Jensen, J. F. Sherson, A. S. Sørensen, and E. S. Polzik, Spin squeezing of atomic ensembles via nuclear-electronic spin entanglement, *Physical review letters* **101**, 073601 (2008).
- [39] D. Oblak, P. G. Petrov, C. L. G. Alzar, W. Tittel, A. K. Vershovski, J. K. Mikkelsen, J. L. Sørensen, and E. S. Polzik, Quantum-noise-limited interferometric measurement of atomic noise: Towards spin squeezing on the cs clock transition, *Physical Review A* **71**, 043807 (2005).
- [40] M. Saffman, D. Oblak, J. Appel, and E. Polzik, Spin squeezing of atomic ensembles by multicolor quantum nondemolition measurements, *Physical Review A* **79**, 023831 (2009).
- [41] E. S. Polzik and J. Ye, Entanglement and spin squeezing in a network of distant optical lattice clocks, *Physical Review A* **93**, 021404 (2016).
- [42] Z. Chen, J. G. Bohnet, J. M. Weiner, K. C. Cox, and J. K. Thompson, Cavity-aided nondemolition measurements for atom counting and spin squeezing, *Physical Review A* **89**, 043837 (2014).
- [43] S. De Echaniz, M. W. Mitchell, M. Kubasik, M. Koschorreck, H. Crepaz, J. Eschner, and E. S. Polzik, Conditions for spin squeezing in a cold 87rb ensemble, *Journal of Optics B: Quantum and Semiclassical Optics* **7**, S548 (2005).
- [44] G. Vitagliano, G. Colangelo, F. M. Ciurana, M. W. Mitchell, R. J. Sewell, and G. Tóth, Entanglement and extreme planar spin squeezing, *Physical Review A* **97**, 020301 (2018).
- [45] M. Wang, W. Qu, P. Li, H. Bao, V. Vuletić, and Y. Xiao, Two-axis-twisting spin squeezing by multipass quantum erasure, *Physical Review A* **96**, 013823 (2017).
- [46] E. Pedrozo-Peñafiel et al., Entanglement on an optical atomic-clock transition, *Nature* **588**, 414 (2020).
- [47] S. Colombo, E. Pedrozo-Peñafiel, A. F. Adiyatullin, Z. Li, E. Mendez, C. Shu, and V. Vuletić, Time-reversal-based quantum metrology with many-body entangled states, *Nature Physics* **18**, 925 (2022).
- [48] B. K. Malia, Y. Wu, J. Martínez-Rincón, and M. A. Kasevich, Distributed quantum sensing with mode-entangled spin-squeezed atomic states, *Nature* **612**, 661 (2022).
- [49] Y. Zhao, Y. Okawachi, J. K. Jang, X. Ji, M. Lipson, and

- A. L. Gaeta, Near-degenerate quadrature-squeezed vacuum generation on a silicon-nitride chip, *Physical Review Letters* **124**, 193601 (2020).
- [50] W. J. Eckner, N. D. Oppong, A. Cao, A. W. Young, W. R. Milner, J. M. Robinson, J. Ye, and A. M. Kaufman, Realizing spin squeezing with rydberg interactions in a programmable optical clock, *arXiv preprint arXiv:2303.08078* (2023).
- [51] Z. Chen, J. G. Bohnet, S. R. Sankar, J. Dai, and J. K. Thompson, Conditional spin squeezing of a large ensemble via the vacuum rabi splitting, *Physical review letters* **106**, 133601 (2011).
- [52] B. Braverman, A. Kawasaki, E. Pedrozo-Peñafiel, S. Colombo, C. Shu, Z. Li, E. Mendez, M. Yamoah, L. Salvi, D. Akamatsu, Y. Xiao, and V. Vuletić, Near-unitary spin squeezing in yb 171, *Physical review letters* **122**, 223203 (2019).
- [53] T. Tashima, T. Wakatsuki, Ş. K. Özdemir, T. Yamamoto, M. Koashi, and N. Imoto, Local transformation of two einstein-podolsky-rosen photon pairs into a three-photon w state, *Physical review letters* **102**, 130502 (2009).
- [54] H. Mikami, Y. Li, K. Fukuoka, and T. Kobayashi, New high-efficiency source of a three-photon w state and its full characterization using quantum state tomography, *Physical review letters* **95**, 150404 (2005).
- [55] B. Fang, M. Menotti, M. Liscidini, J. Sipe, and V. Lorenz, Three-photon discrete-energy-entangled w state in an optical fiber, *Physical review letters* **123**, 070508 (2019).
- [56] M. Eibl, N. Kiesel, M. Bourennane, C. Kurtsiefer, and H. Weinfurter, Experimental realization of a three-qubit entangled w state, *Physical review letters* **92**, 077901 (2004).
- [57] R. J. Sewell, M. Koschorreck, M. Napolitano, B. Dubost, N. Behbood, and M. W. Mitchell, Magnetic sensitivity beyond the projection noise limit by spin squeezing, *Physical review letters* **109**, 253605 (2012).
- [58] M. Koschorreck, M. Napolitano, B. Dubost, N. Behbood, R. Sewell, and M. W. Mitchell, Spin squeezing via quantum non-demolition measurements in cold 87rb atomic ensemble, in *Quantum Electronics and Laser Science Conference* (Optica Publishing Group, 2010) p. QThA4.
- [59] A. Omran et al., Generation and manipulation of schrödinger cat states in rydberg atom arrays, *Science* **365**, 570 (2019).
- [60] Y.-F. Huang, B.-H. Liu, L. Peng, Y.-H. Li, L. Li, C.-F. Li, and G.-C. Guo, Experimental generation of an eight-photon greenberger-horne-zeilinger state, *Nature communications* **2**, 546 (2011).
- [61] X. Su, A. Tan, X. Jia, J. Zhang, C. Xie, and K. Peng, Experimental preparation of quadripartite cluster and greenberger-horne-zeilinger entangled states for continuous variables, *Physical review letters* **98**, 070502 (2007).
- [62] K. Takeda, A. Noiri, T. Nakajima, J. Yoneda, T. Kobayashi, and S. Tarucha, Quantum tomography of an entangled three-qubit state in silicon, *Nature Nanotechnology* **16**, 965 (2021).
- [63] R. H. Dicke, Coherence in spontaneous radiation processes, *Physical review* **93**, 99 (1954).
- [64] R. M. Kroeze, B. P. Marsh, K.-Y. Lin, J. Keeling, and B. L. Lev, High cooperativity using a confocal-cavity-qed microscope, *PRX Quantum* **4**, 020326 (2023).
- [65] J. Huo et al., Gatemon qubit based on a thin inas-al hybrid nanowire, *Chinese Physics Letters* **40**, 047302 (2023).
- [66] C. Rigetti et al., Superconducting qubit in a waveguide cavity with a coherence time approaching 0.1 ms, *Physical Review B* **86**, 100506 (2012).
- [67] S. Chakram, A. E. Orian, R. K. Naik, A. V. Dixit, K. He, A. Agrawal, H. Kwon, and D. I. Schuster, Seamless high-q microwave cavities for multimode circuit quantum electrodynamics, *Physical review letters* **127**, 107701 (2021).
- [68] O. Milul, B. Guttel, U. Goldblatt, S. Hazanov, L. M. Joshi, D. Chausovsky, N. Kahn, E. Çiftçiyörek, F. Lafont, and S. Rosenblum, Superconducting cavity qubit with tens of milliseconds single-photon coherence time, *PRX Quantum* **4**, 030336 (2023).
- [69] H. Tanji-Suzuki, I. Leroux, M. Schleier-Smith, M. Cetina, A. Grier, J. Simon, and V. Vuletić, *Advances in atomic, molecular, and optical physics* (2011).
- [70] Y. Zhao, R. Zhang, W. Chen, X.-B. Wang, and J. Hu, Creation of greenberger-horne-zeilinger states with thousands of atoms by entanglement amplification, *NPJ Quantum Information* **7**, 24 (2021).
- [71] D. J. Wineland, J. J. Bollinger, W. M. Itano, F. Moore, and D. J. Heinzen, Spin squeezing and reduced quantum noise in spectroscopy, *Physical Review A* **46**, R6797 (1992).
- [72] M. Kitagawa and M. Ueda, Squeezed spin states, *Physical Review A* **47**, 5138 (1993).
- [73] S. Lloyd, Almost any quantum logic gate is universal, *Physical review letters* **75**, 346 (1995).
- [74] G. Kimura, The bloch vector for n-level systems, *Physics Letters A* **314**, 339 (2003).
- [75] Z. Li, B. Braverman, S. Colombo, C. Shu, A. Kawasaki, A. F. Adiyatullin, E. Pedrozo-Peñafiel, E. Mendez, and V. Vuletić, Collective spin-light and light-mediated spin-spin interactions in an optical cavity, *PRX Quantum* **3**, 020308 (2022).
- [76] Optimized data and necessary code, https://github.com/ZhangTao1999/Entanglement_generation_via_single_qubit_operation_in_a_teaared_Hilbert_space (2023), accessed: December 7, 2023.